

Radiation-MHD models of elephant trunks and globules in H II regions

Jonathan Mackey^{1,2*} and Andrew J. Lim¹

¹ Dublin Institute for Advanced Studies, 31 Fitzwilliam Place, Dublin 2, Ireland

² Argelander Institut für Astronomie, Auf dem Hügel 71, 53121 Bonn, Germany

Abstract: We study the formation and evolution of pillars of dense gas, known as elephant trunks, at the boundaries of H II regions, formed by shadowing of ionising radiation by dense clumps. The effects of magnetic fields on this process are investigated using 3D radiation-magnetohydrodynamics simulations. For a simulation in which an initially uniform magnetic field of strength $|\mathbf{B}| \simeq 50 \mu\text{G}$ is oriented perpendicular to the radiation propagation direction, the field is swept into alignment with the pillar during its dynamical evolution, in agreement with observations of the “Pillars of Creation” in M16, and of some cometary globules. This effect is significantly enhanced when the simulation is re-run with a weaker field of $\simeq 18 \mu\text{G}$. A stronger field with $|\mathbf{B}| \simeq 160 \mu\text{G}$ is sufficient to prevent this evolution completely, also significantly affecting the photoionisation process. Using a larger simulation domain it is seen that the pillar formation models studied in Mackey & Lim (2010) ultimately evolve to cometary structures in the absence of dense gas further from the star.

1 Introduction

The interstellar magnetic field in the Eagle Nebula (M16) was measured by Sugitani et al. (2007) using near infrared polarisation observations of background stars. They found that the field orientation within the massive pillars of gas and dust in M16 (Hester et al. 1996), known as the “Pillars of Creation”, is aligned with the long axis of the pillars and with the UV radiation propagation direction, but misaligned with the ambient magnetic field (see Fig. 3 below). If the pillars have formed dynamically due to shadowing of ionising radiation (e.g. Williams, Ward-Thompson & Whitworth 2001; Lim & Mellema 2003) then it appears the field has been re-oriented by this process. Sugitani et al. (2007) suggest that this may constrain the ambient field strength in M16 because ionised gas pressure appears to dominate the dynamics. Here we test this suggestion and build on our earlier non-magnetised results (Mackey & Lim 2010, hereafter ML10) by using 3D radiation-magnetohydrodynamics (R-MHD) simulations to model the formation of pillars and globules due to shadowing of ionising radiation by pre-existing dense clumps.

A uniform grid, 2nd order accurate, finite volume code (see ML10) is used for the MHD calculations with a Roe-type Riemann solver (Cargo & Gallice 1997). The short characteristics ray-tracer is used to track direct monochromatic ionising radiation and the on-the-spot approximation for diffuse radiation. Radiative cooling is calculated explicitly for recombining hydrogen and using a cooling

*jmackey@astro.uni-bonn.de

Table 1: Simulation parameters for model R5, showing grid resolution (zones), domain coordinates in parsecs (\mathbf{X}_{\min} , \mathbf{X}_{\max}) relative to the radiation source which has monochromatic photon luminosity and photon energy as indicated. Clump positions, peak number density (n_{H}), Gaussian scale radius (r_0) and total mass (M) are as indicated; the background magnetic field (in μG), number density (n_{H}) and gas pressure (p_g) are similarly indicated.

Name	x	y	z	Further information.
Zones	384	256	256	Uniform Cartesian grid.
\mathbf{X}_{\min}	1.5	-1.5	-1.5	position in parsecs relative to the source.
\mathbf{X}_{\max}	6.0	1.5	1.5	position in parsecs relative to the source.
Source	0	0	0	$L_{\gamma} = 2 \times 10^{50} \text{ s}^{-1}$, $h\nu_0 = 13.6 \text{ eV} = 5.0 \text{ eV}$
Clump 1	2.30	0	0	$n_{\text{H}} = 10^5 \text{ cm}^{-3}$, $r_0 = 0.09 \text{ pc}$, $M = 28.4 M_{\odot}$
Clump 2	2.75	0	0.12	$n_{\text{H}} = 10^5 \text{ cm}^{-3}$, $r_0 = 0.09 \text{ pc}$, $M = 28.4 M_{\odot}$
Clump 3	3.20	0	-0.12	$n_{\text{H}} = 10^5 \text{ cm}^{-3}$, $r_0 = 0.09 \text{ pc}$, $M = 28.4 M_{\odot}$
Background	$\mathbf{B}_0 = [0, 0, 53]$			$n_{\text{H}} = 200 \text{ cm}^{-3}$, $p_g = 1.38 \times 10^{-11} \text{ dyne cm}^{-2}$

curve for other elements, with neutral/molecular gas cooling treated very approximately by exponential cooling with cooling time $t_c = 10 \text{ kyr}$ (see ML10, cooling model C2). This code has been extensively tested¹ and checked for consistency with previous work (e.g. Falle, Komissarov, & Joarder 1998; Lim & Mellema 2003; Mellema et al. 2006; Krumholz, Stone, & Gardiner 2007; Henney et al. 2009, ML10 and references therein).

2 Simulations

We have performed a number of 3D R-MHD simulations, to be presented in more detail in Mackey & Lim (2011). Here we present results from one of the simulations, denoted R5. This model consists of a monochromatic point source of ionising photons placed 2.3 pc from the nearest of three dense gas clumps (Gaussian density profiles) in a uniform background medium ($n_{\text{H}} = 200 \text{ cm}^{-3}$). Simulation parameters are described in Table 1; the same model was presented on a smaller simulation domain with zero field in ML10 but here a uniform magnetic field of $\mathbf{B} = [0, 0, 53] \mu\text{G}$ is imposed in the initial conditions.

The evolution of dense gas over 400 kyr is shown in Fig. 1, where the initial field is horizontal and in the plane of the images. The evolution is broadly similar to that of the R-HD model in ML10 for the first $\sim 250 \text{ kyr}$, but there are notable differences. Radiation-driven implosion ($t \sim 100 \text{ kyr}$) is more pronounced along field lines than across them, leading to a flattened structure (cf. Henney et al. 2009); the narrow tail in the second panel is actually a sheet seen edge-on and the clumps are also flattened. Following this (200 – 300 kyr) magnetic pressure generates a stronger re-expansion and hence the pillar/globule is larger and has a lower density than the R-HD case. The re-expansion leads to fragmentation in this model ($t \gtrsim 400 \text{ kyr}$), just beginning in the right-most panel. It is seen that the simulation ultimately evolves from being pillar-like (dense elongated structure) to a cometary globule (dense flattened head, low density neutral tail) in the absence of dense gas further from the star. We have confirmed that this is also true when the model is run with zero magnetic field (i.e. identical to model 17 in ML10 but with a larger simulation domain).

¹For more information, including test results, see <http://www.astro.uni-bonn.de/~jmackey/jmac/>.

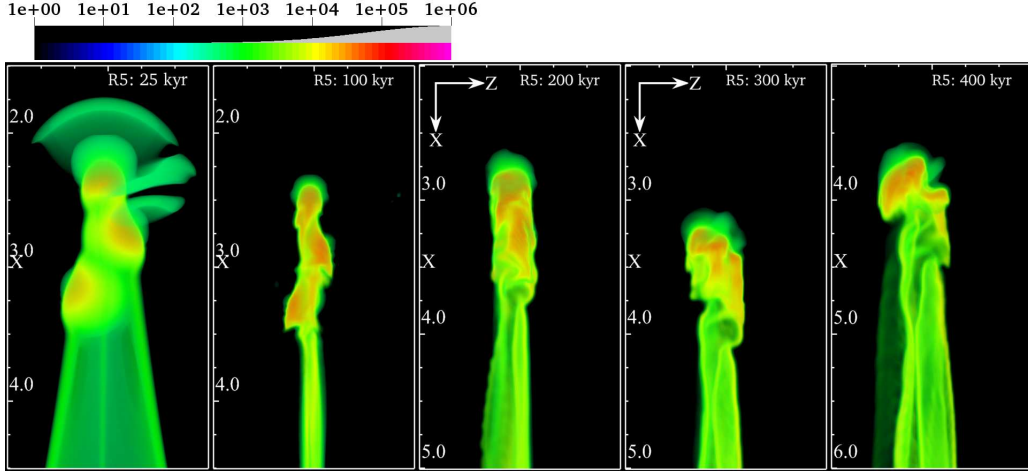


Figure 1: Volume-rendered images of gas density in the 3D R-MHD simulation R5 described above, shown at times $t = 25, 100, 200, 300, 400$ kyr. Tick-marks at 0.25 pc intervals show the physical scale (numbers refer to the tick-marks immediately below them). The logarithmic number density scale (cm^{-3}) is shown above, with the opacity function used for image generation as the grey curve (gas with $n_{\text{H}} \lesssim 10^3 \text{ cm}^{-3}$ is transparent). Only part of the simulation domain is shown in each panel.

3 Discussion

The projected magnetic field orientation was calculated by a density-weighted integration of “Stokes parameters” Q and U for the perpendicular magnetic field along the lines of sight (LOS) (cf. Arthur et al. 2010):

$$\langle Q \rangle = \int_{z=0}^{\infty} \min[n_{\text{H}}(z), n_{\text{max}}] \frac{B_x^2 - B_y^2}{\sqrt{B_x^2 + B_y^2}} dz, \quad \langle U \rangle = \int_{z=0}^{\infty} \min[n_{\text{H}}(z), n_{\text{max}}] \frac{2B_x B_y}{\sqrt{B_x^2 + B_y^2}} dz, \quad (1)$$

with $n_{\text{max}} = 2.5 \times 10^4 \text{ cm}^{-3}$. Here $x - y$ is the image plane and z is distance along the LOS (i.e. observer rather than simulation coordinates). The projected field is then recovered from $\langle Q \rangle$ and $\langle U \rangle$ using trigonometric relations.

Formally this has units of $\mu\text{G cm}^{-2}$, but the normalisation is irrelevant for the orientation. The projected field orientation is over-plotted on column density maps in Fig. 2, projected such that the initial field is fully in the image plane and vertical. At $t = 250$ kyr the clumps have undergone significant dynamical evolution and the pillar-like structure is slowly being flattened due to the rocket effect. The magnetic field, while relatively unaffected in ionised gas and the low density tail region, has clearly been dragged into alignment with the pillar in dense gas due to the pillar’s acceleration away from the star. At 400 kyr only a flattened cometary globule remains, but the field is even more strongly aligned with the acceleration direction. This clearly shows that an initially perpendicular field is swept into alignment with the pillar during its dynamical evolution, and that this alignment remains once the structure evolves to a cometary morphology. This is in agreement with the observations of the pillars in M16 (reproduced here in Fig. 3, Sugitani et al. 2007) and some cometary globules (e.g. Bhatt, Maheswar, & Manoj, 2004) which also have the field aligned with the cometary tail.

The behaviour of the same simulation with a magnetic field $3\times$ weaker (R2) and $3\times$ stronger (R8) is rather different however (to be discussed in more detail in Mackey & Lim 2011). For R2 with $B \simeq 18 \mu\text{G}$ the field is more easily deformed by photoionisation-induced gas motions and the alignment is even stronger, whereas for R8 with $B \simeq 160 \mu\text{G}$ the field is dynamically dominant and barely changes from its initial perpendicular state. This is shown in the right panel of Fig. 3 where the ratio of the volume averaged field parallel and perpendicular to the radiation propagation

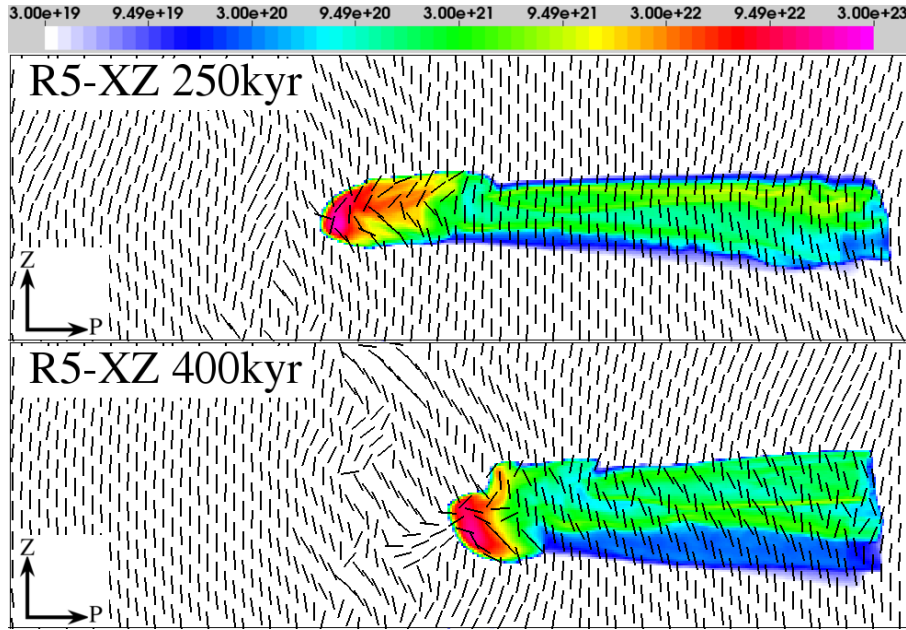


Figure 2: Column density (colour scale in cm^{-2}) and projected magnetic field (lines show orientation only) for the R5 simulation at 250 kyr (above) and 400 kyr (below). The projection LOS is $\hat{n} = \hat{x} \sin(20^\circ) + \hat{y} \cos(20^\circ)$ in the simulation coordinate system, so the initial magnetic field ($\mathbf{B} = 53\hat{z} \mu\text{G}$) is vertical and \perp to the LOS. The horizontal axis labelled P is therefore $\hat{P} = \hat{x} \cos(20^\circ) - \hat{y} \sin(20^\circ)$ i.e. a 20° rotation from the x -axis about the z -axis.

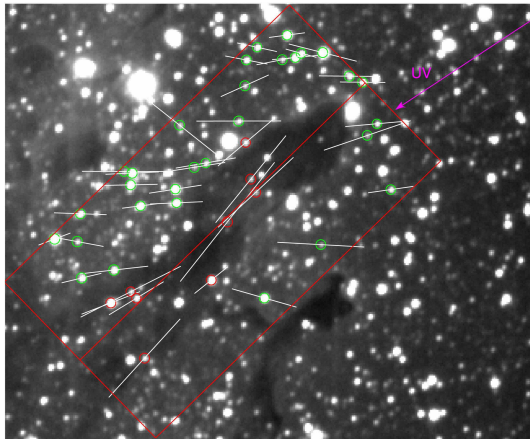


Figure 3: Figure 9b from Sugitani et al. (2007) showing near-IR absorption polarimetry observations of the magnetic field orientation in the central pillar in M16 (© the Astronomical Society of Japan; used with permission). North is to the top, East to the left, and the image width is $\simeq 2'.5$.

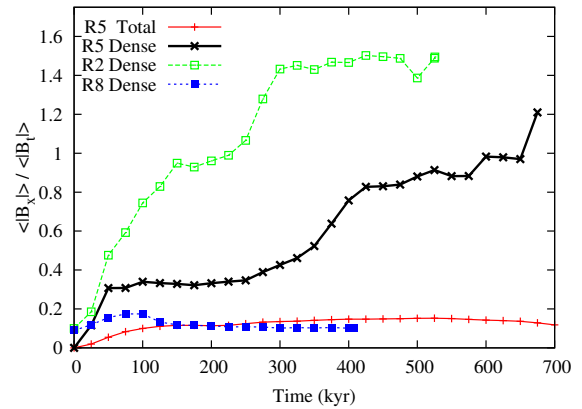


Figure 4: Ratio of volume-averaged parallel field $\langle |B_x| \rangle$ to perpendicular field $\langle \sqrt{B_y^2 + B_z^2} \rangle$ as a function of time in simulations R2, R5, and R8. Red line: average of all cells (R5); Black: average of only dense cells with $n_{\text{H}} > 5000 \text{ cm}^{-3}$ (R5); Green: simulated with $|\mathbf{B}|$ $3\times$ weaker (R2); Blue: with $|\mathbf{B}|$ $3\times$ stronger (R8).

direction (\hat{x}) are plotted as a function of time for R2, R5, and R8. The evolution of dense gas with $n_{\text{H}} > 5000 \text{ cm}^{-3}$ is shown for all three models, and for the full simulation volume only for R5 (R2 and R8 are very similar). It is seen that while the ratio does not evolve significantly when averaged over the full simulation volume, in dense gas the situation is very different. For R5 the parallel field increases rapidly during the implosion phase and there is a subsequent slower increase during the acceleration phase to roughly equal field strength in both components. This trend is stronger for the weak field model R2, whereas for the strong field model R8 the field orientation remains almost constant throughout the simulation. This difference between the weaker and stronger field simulations is larger than was found by Henney et al. (2009) and deserves further investigation.

4 Conclusions

The results presented here show that both radiation-driven implosion and acceleration of clumps by the rocket effect tend to align the magnetic field with the radiation propagation direction in dense neutral gas. As was suggested by Sugitani et al. (2007), the effectiveness of this alignment is dependent on the initial field strength. For simulations which have similar gas densities and pressures to conditions in M16, we have shown that a magnetic field of strength $\sim 160 \mu\text{G}$ is sufficient to prevent any significant field reorientation. These results suggest that an ambient field of $|\mathbf{B}| < 160 \mu\text{G}$ (and more likely $|\mathbf{B}| \sim 50 \mu\text{G}$) is required to explain the observed field configuration in the M16 pillars if the pillars formed via the mechanism we are modelling. Detailed R-HD models have recently been performed with dynamic initial conditions (Gritschneder et al. 2010) rather than the initially static models of ML10, allowing a potentially more realistic comparison with observations. Addition of magnetic fields to their simulations would be very useful to assess how significantly a non-uniform initial magnetic field will impact on the results presented here.

Acknowledgements

JM acknowledges funding for this work from the Irish Research Council for Science, Engineering and Technology; from the Dublin Institute for Advanced Studies; and from Science Foundation Ireland. AJL's work has been funded by a Schrödinger Fellowship from the Dublin Institute for Advanced Studies. The authors wish to acknowledge the SFI/HEA Irish Centre for High-End Computing (ICHEC) for the provision of computational facilities and support. Fig. 9b from Sugitani et al. (2007) © The Astronomical Society of Japan; reproduced with permission.

References

- Arthur S. J., Henney W. J., Mellema G., De Colle F., Vázquez-Semadeni E., 2010, MNRAS, submitted.
Bhatt, H. C., Maheswar, G., & Manoj, P. 2004, MNRAS, 348, 83
Cargo, P., & Gallice, G. 1997, Journal of Computational Physics, 136, 446
Falle, S., Komissarov, S., & Joarder, P. 1998, MNRAS, 297, 265
Gritschneder, M., Burkert, A., Naab, T., & Walch, S. 2010, ApJ, 723, 971
Henney, W. J., Arthur, S. J., de Colle, F., & Mellema, G. 2009, MNRAS, 398, 157
Hester, J. J., Scowen, P. A., Sankrit, R., et al. 1996, AJ, 111, 2349
Krumholz, M., Stone, J., & Gardiner, T. 2007, ApJ, 671, 518
Lim, A., & Mellema, G. 2003, A&A, 405, 189
Mackey, J., & Lim, A. J. 2010, MNRAS, 403, 714
Mackey, J., & Lim, A. J. 2011, in preparation
Mellema, G., Iliiev, I., Alvarez, M., & Shapiro, P. 2006, New Astronomy, 11, 374
Sugitani, K., Watanabe, M., Tamura, M., et al. 2007, PASJ, 59, 507
Williams, R., Ward-Thompson, D., & Whitworth, A. 2001, MNRAS, 327, 788